ResearchGate

See discussions, stats, and author profiles for this publication at: https://www.researchgate.net/publication/362940077

Finite Element Analysis on AISI 316L Stainless Steel Exposed to Ball-on-Flat Dry Sliding Wear Test

Article *in* Transactions of the Indian Institute of Metals · August 2022

DOI: 10.1007/s12666-022-02720-4

CITATIONS
11

READS
533

4 authors, including:



Juan Carlos Martinez Londoño
San Buenaventura University
5 PUBLICATIONS **93** CITATIONS
SEE PROFILE



J. Martínez-Trinidad
National Polytechnic Institute
67 PUBLICATIONS **1,455** CITATIONS
SEE PROFILE



Ricardo A. García-León
Francisco de Paula Santander University
100 PUBLICATIONS **899** CITATIONS
SEE PROFILE

All content following this page was uploaded by Ricardo A. García-León on 03 September 2023.

The user has requested enhancement of the downloaded file.

Trans Indian Inst Met
https://doi.org/10.1007/s12666-022-02720-4

ORIGINAL ARTICLE

Finite Element Analysis on AISI 316L Stainless Steel Exposed to Ball-on-Flat Dry Sliding Wear Test

J. C. Martínez-Londoño[1] · J. Martínez-Trinidad[1] · A. Hernández-Fernández[1] · R. A. García-León[2]

Received: 2 March 2022 / Accepted: 25 July 2022
© The Indian Institute of Metals - IIM 2022

Abstract A finite element analysis model is presented in this work by implementing the UMESHMOTION subroutine in the software suite ABAQUS, simulating the sliding wear in a configuration ball-on-flat on an AISI 316L. The model is based on an arbitrary Lagrangian–Eulerian (ALE) remeshing technique implementing a modified Archard's equation. In the model, shape functions and Newton–Raphson formulation were implemented to find the contact pressure and sliding values on the sample and thus validate the wear depth with those reported in the literature. A mesh independence analysis was developed, taking into account contact element size, discretization in the total number of cycles, and the maximum step increment. The contact pressure after the initial loading was calculated and compared with values found by Hertzian formulation found in the literature having a maximum error of 8.61%. Wear depth found was in good agreement with the values reported in the literature, with a maximum error of 18.77%.

Keywords Wear · FEM · Stainless steel · ABAQUS · UMESHMOTION

✉ J. Martínez-Trinidad
jomartinezt@ipn.mx

✉ R. A. García-León
ragarcial@ufpso.edu.co

[1] Instituto Politécnico Nacional, Grupo Ingeniería de Superficies, SEPI-ESIME, U.P. Adolfo López Mateos, Zacatenco, D.F 07738 México, México

[2] Universidad Francisco de Paula Santander Ocaña, Grupo de Investigación INGAP, CP 546552 Ocaña, Colombia

1 Introduction

Sliding wear is a general term used to describe the contact of two surfaces that slides without the presence of particles between the surfaces. The material loss between the surfaces is known as wear. Wear is a complex process controlled by the stress and mechanical damage, thermal effects, chemical reactions, and interactions of the surfaces [1]. The geometry of the samples is one of the main aspects in a sliding wear test; ball-on-flat configuration has been used in several wear studies [2–4].

Finite element models have been successfully implemented to simulate contact and wear material losses [5–8]. Hegadekatte et al. [9] used a post-processor together with the FEM software ABAQUS to model a 2D pin-on-disk configuration using Archard's law to compute the wear progress. The results evidence that Archard's wear model is valid on both sides on the global and local scale in the particular case when the materials are stiff. Kanavalli B [10] proposed the implementation of ABAQUS subroutine UMESHMOTION to simulate a twin-disk tribometer, concluding that the subroutine can be coded to simulate rolling/sliding wear in a twin-disk tribometer. On the other hand, Hegadekatte et al. [11] compared the post-processor and the UMESHMOTION models and found that both have acceptable accuracies to model sliding wear.

Using a special-purpose FORTRAN program and ABAQUS, McColl et al. [12] simulated the fretting wear in a cylinder-on-flat fretting configuration. The predicted wear scars were compared with profilometer measurements of fretting test scars. The results exposed that the measured and predicted worn surface profiles correlated well for the low normal load case, but under high normal loads, the predicted maximum wear depth was under-estimated, and the width of the scar was over-estimated. Kunal and Ramkumar

Published online: 25 August 2022

[13] used a 2D FEM to model dry sliding abrasive wear using ALE remeshing with UMESHMOTION subroutine on the finite element software ABAQUS, founding significant errors at high loads between the hertz formulation and the modeled contact pressure. The model was validated using the wear depth for experimental data for normal force 10 N.

Considering the models used to calculate the wear process on an AISI 316L stainless steel under ball-on-flat dry sliding conditions, Archard's law is implemented using arbitrary Lagrangian–Eulerian (ALE) remeshing with UMESHMOTION subroutine on the finite element software ABAQUS. Similar works can be found in different geometries like a cylinder on flat and pin on disk, but the authors do not know a 3D implementation on ball-on-flat geometry. The model is validated using the experimental result from García-León et al. [2]. Nowadays, the majority of finite element software does not allow the direct modeling of wear since the software does not give information about material loss and the subsequent geometry variation. To avoid this problem, the implemented model uses a static formulation with an ALE remeshing technique using UMESHMOTION subroutines to define the wear in the contact surfaces. The ALE remeshing is updated at the end of every step of the analysis and the wear is included at this stage; the remeshing technique avoids the over deformation of the elements without creating new elements in the domain.

2 Materials and Methods

2.1 Archard's Wear Formulation

Many factors are important in wear including the material properties, the geometry of the wearing bodies, operational and environmental variables, however the material loss is usually estimated using simplified formulations. These formulations have the advantage to find good wear estimation values without the need to solve high complexity equations or the need of high computational power models, at the cost that the formulation cannot be indiscriminately used in all the test configurations and materials.

Archard's law relates Q the volume worn per unit sliding distance(mm^3/mm), with the macroscopic quantities, W the normal load (N), H the hardness of the softer material (N/mm^2), and the dimensionless constant K commonly known as wear coefficient [1], as shown in Eq. (1). In this equation, the wear loss is only related to the softer material hardness and is often consistent with experimental observations in metals.

$$Q = \frac{K \times W}{H} \tag{1}$$

Equation (1) is intended to be used on the global scale, dividing by the contact area and discretizing with respect to the sliding distance Archard's law can be written as shown in Eq. (2).

$$\frac{\mathrm{d}h}{\mathrm{d}s} = k_D \times P \tag{2}$$

where P is the contact pressure (N/mm^2), h is the total wear (mm), k_D is the dimensional wear coefficient (mm^3/Nm), and s is the sliding distance (mm). This equation can be integrated using the Euler integration scheme to obtain an expression that can be used in the local scale, as seen in Eq. (3).

$$h_{i+1} = h_i + \left(k_D \times P_i \times \mathrm{d}s\right) \tag{3}$$

where h_{i+1} is the total wear up to the $i+1$ increment, h is the total wear up to the I increment, P_i is the contact pressure during the i increment and ds is the slipping of the current node.

2.2 UMESHMOTION Implementation ABAQUS

ALE adaptive meshing is a tool that can be used to maintain a high-quality mesh even with high deformation and material loss; by allowing the mesh to move independently from the material [14], adaptive meshing is effective for simulations of metal forming processes such as forging, extrusion and rolling but it has been successfully implemented together with UMESHMOTION subroutine to model wear [10, 11]. UMESHMOTION is a user-defined subroutine where the motion of nodes in an ALE adaptive meshing can be defined [15]. The overall methodology for the UMESHMOTION implementation can be found in Fig. 1.

2.3 FEM Model

The selected geometry is a ball-on-flat configuration, as shown in Fig. 2a. This geometry is selected to replicate the experimental setup described by García-León et al. [2]. The radius of the ball is 3.0 mm and is located at 1.5 mm from the back face of the sample, and the sample dimensions are reduced, with the aim to decrease the computational requirements of the model. The sample and the ball are divided as shown in Fig. 2a and b to allow a refined element size in the contact zone. C3D8 eight nodes brick elements were used in the entire sample and in the contact zone of the ball. The size of the contact elements will be "Telem,". C3D4 elements were used in the outer part of the ball, the dimension of the contact zones of the sample and the ball are proximal to $0.75 \times 1.2 \times 0.12$ mm. The contact zones are connected to the outer parts using a Tie constrain.

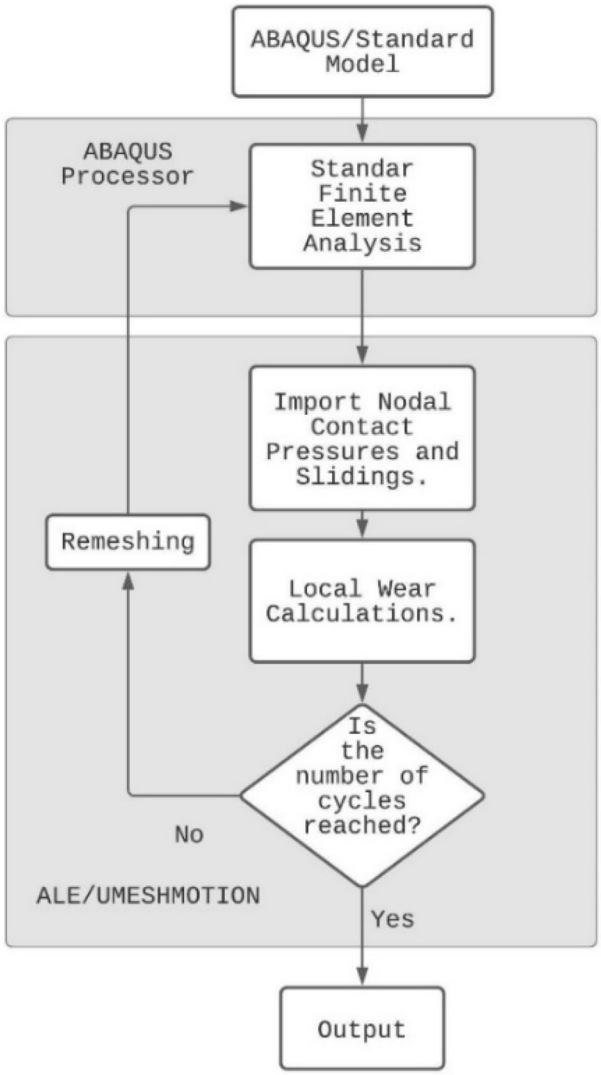


Fig. 1 UMESHMOTION Implementation flowchart. *Source* Authors

The AISI 316L sample is modeled as an elastic isotropic material with young modulus 210 GPa, Poisson ratio 0.27, and density 7.9×10^{-8} kg/mm^3. The alumina ball is modeled as an elastic isotropic material with young modulus 350 GPa, Poisson ratio 0.3, and density 3.96×10^{-8} kg/mm^3 [16]. To model the sample is contradictory to the fact that the damage to the wearing surface and thus the material loss during abrasive wear are results when the plastic strain at the subsurface accumulates and reaches a critical value for fracture [17], especially in early stages when the scar has not yet formed and the contact area will be lesser. But the contact area will increase making the plastic deformation less likely as the wear scar increases its size; also as described in the ASTM G133 the wear volume is computed from the length of the stroke and the average cross-sectional area of the wear track. This volume will also compute the possible deformation from plastic behavior of the sample, so that it will be implicit in the wear coefficient. Modeling the sample as an elastoplastic material will show a better fitting to the real model, but the inclusion of the plastic behavior in the model will increase the computational power needed and cause divergence in the solution algorithm.

The model is intended to simulate a total of 5000 cycles, the same number of cycles that [2] exist in their experimental setup. The computational power needed to solve all the 5000 cycles is a restriction to the analysis. So the model was divided into several steps, each of them simulating "DN" cycles. As a consequence, a total of 5000/DN steps will be needed to simulate the sliding phase of the model. The DN parameter has the same characteristic as that of the constant pressure extrapolation coefficient used by Kunal and Ramkumar [13]. Before the sliding steps, an initial step where the normal load is applied is implemented. After the sliding steps two steps are added, the first one where all the loads are retired and the second one where the ball is moved away from the sample. To implement this discretization of the steps in the model, Eq. (3) can be modified as shown in Eq. (4).

$$h_{i+1} = h_i + \left(\mathrm{DN} \times k_D \times P_i \times \mathrm{d}s\right) \tag{4}$$

The contact between the sample and the alumina ball is defined as a penalty-based Surface to Surface formulation with a tolerance for adjustment of 1×10^{-6} mm. The friction coefficient has been fixed at 0.65. The master surface is defined as the alumina ball. The contact pressure and sliding values on the sample are interpolated from the closest four nodes of the alumina ball using shape functions and a multivariable Newton–Raphson to solve the resulting equation system.

Displacement in all directions and rotation on *Y*-axis was restricted for the bottom face of the sample. The top face of the alumina ball was tied to a reference point where the boundary conditions and loads were applied. The reference point was restricted to move only on the *y*-direction on the loading and unloading steps, and the movement was defined on it for the sliding steps. A schematic for the restriction can be found in Fig. 3a and b. In Fig. 3c and d, it can be appreciated that the contact zone in the model has a much-refined element size (Telem = 0.03 mm). This behavior has been implemented by several authors [3, 9, 17–20]and is needed for the convergence of the model.

Initially, a DN value of 500 cycles and a normal load of 5 N were fixed, and four contact elements were considered. In Fig. 4a, the contact pressure at the end of the loading step versus the number of elements can be seen. As the number of elements increases, the contact pressure has low variability. In Fig. 4b, the maximum wear depth versus the number of elements can be found; it can be concluded that

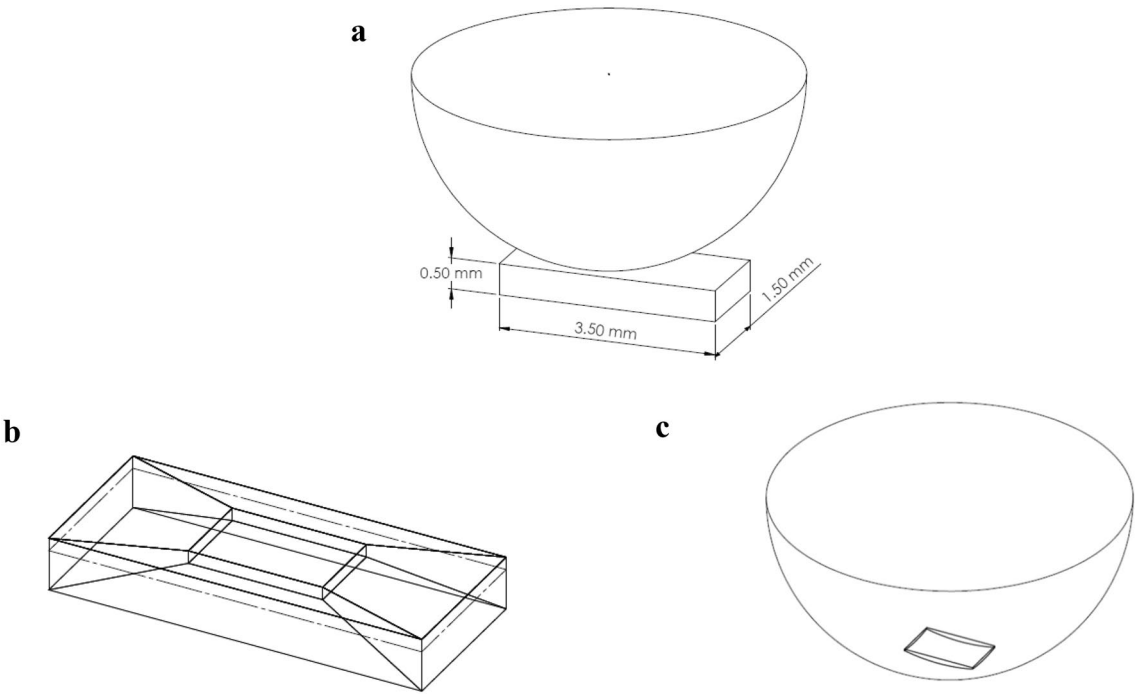


Fig. 2 **a** Example geometry of the model, **b** flat geometry, and **c** alumina ball division for meshing stroke = 0.5 mm

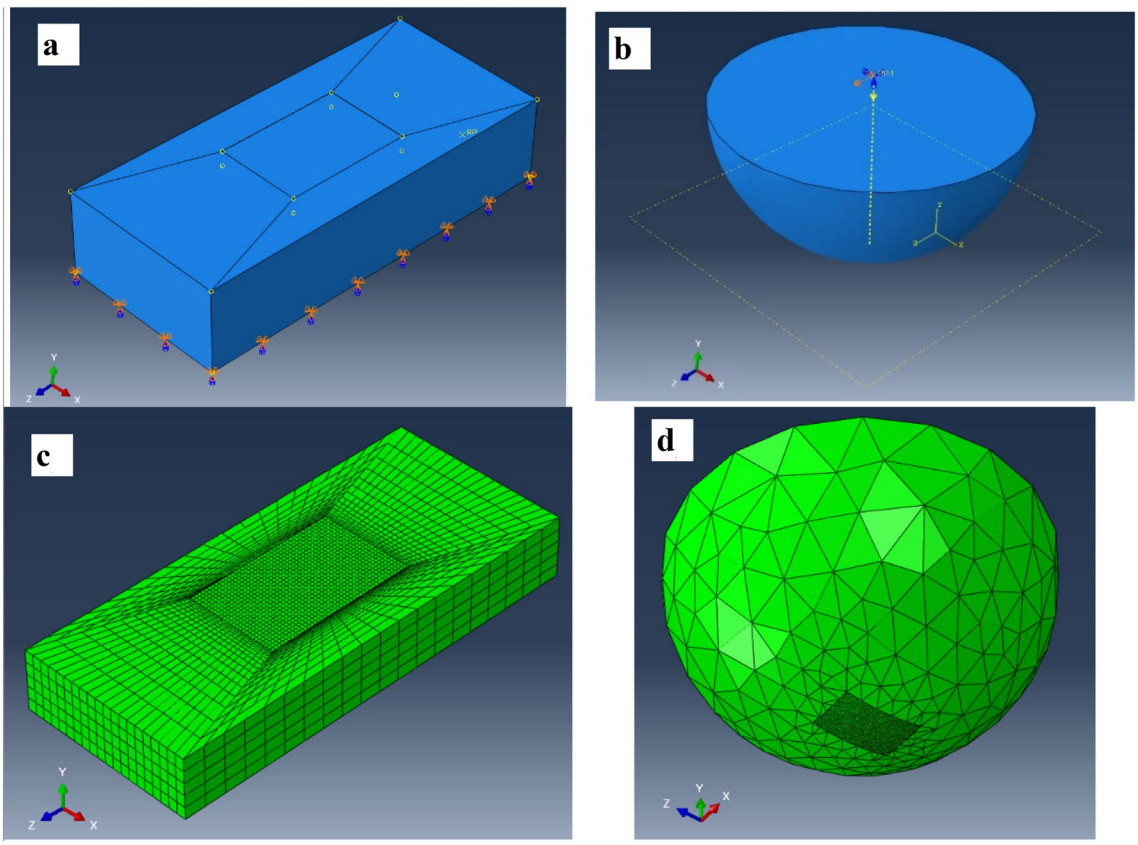


Fig. 3 Boundary conditions for solid geometry: **a** flat and **b** alumina ball. Mesh with Telem = 0.05 mm and stroke = 0.5 mm for **c** flat and **d** alumina ball

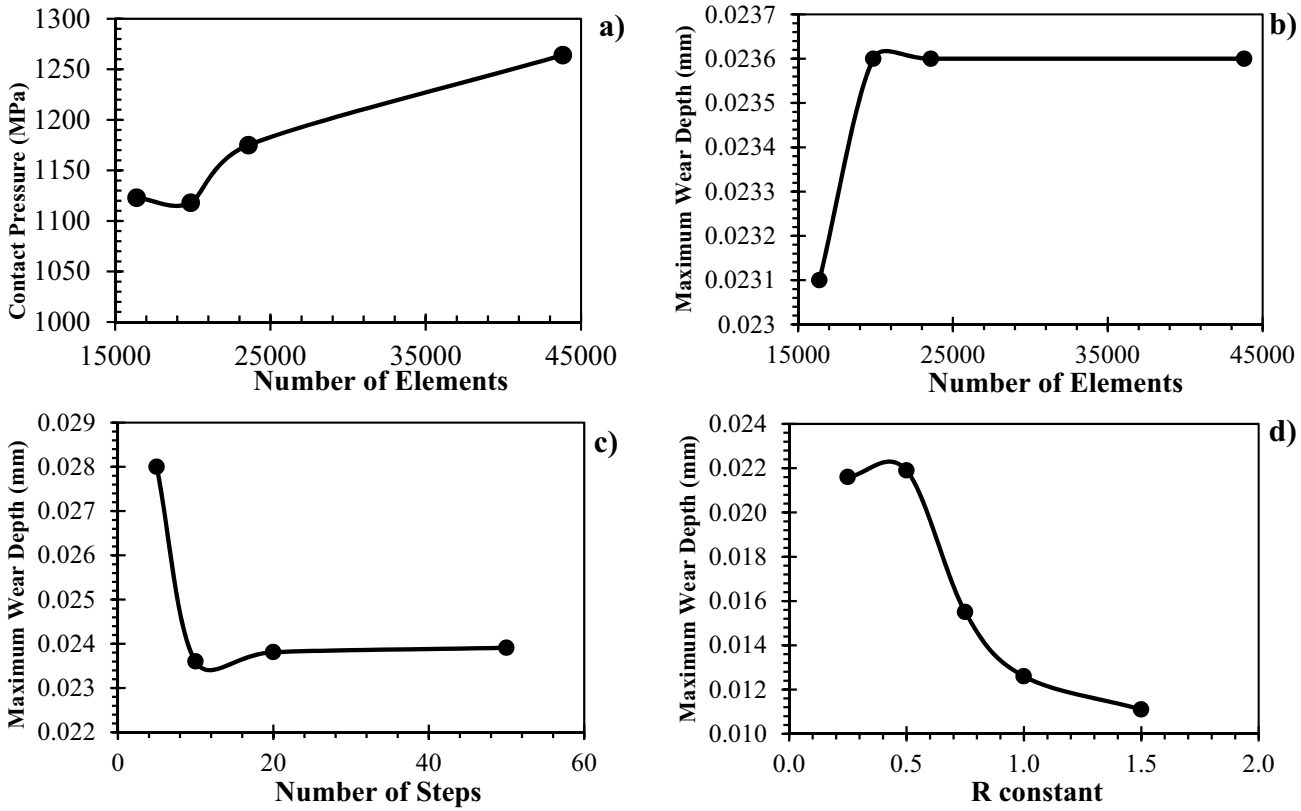


Fig. 4 **a** Contact pressure versus number of elements, **b** maximum wear depth versus number of elements, **c** maximum wear depth versus number of steps and **d** maximum wear depth versus *R* constant. Considering Telem = 0.04 mm, stroke = 0.5 mm, DN = 500 cycles

the wear depth has reached independence from the element size when Telem is approximately 0.04 mm (19,863 elements). With contact element size of 0.04 mm and a stroke value of 0.5 mm, four DN was considered. Figure 4c shows the maximum wear versus the number of steps of the analysis that can be found. It can be concluded that the model will be independent from this variable for a DN value of five hundred cycles (20 steps).

The maximum incrementation time on each of the FEM steps is proportional to the sliding distance increment for each wear step and, as have been reported, is of great significance for the computational expense and the stability of the model [9, 12, 20–22]. An adequate maximum incrementation time must be used as high values can lead to artificial roughening resulting in inconsistent results, and low values will significantly increase the computational model times.

$$\text{IncMax} = \frac{R \times \text{Telem}}{2 \times \text{Stroke}} \tag{5}$$

Equation (5) was used to relate the maximum incrementation time with the element size and the stroke using the constant *R*. In Fig. 4d, the maximum wear depth versus the constant *R* can be found; values of *R* lesser than 0.5 will have a valueless change on the maximum wear depth as can be concluded from the graphic but will reduce the maximum incrementation time and in consequence increase the computational time.

In Fig. 5, the wear scar after the alumina ball retreats as the function of the constant R can be appreciated. At high incrementation time (higher *R* values), the displacement of the nodes in the direction tangential to the contact (U2) displays a significant roughness in the scar, irregularities not expected in the wear model. Between Fig. 5d and e, improvement on the wear scar can be seen, but the computational time required is significantly increased.

3 Results and Discussion

3.1 Model Validation

Table 1 shows the results and experimental conditions obtained by Garcia-Leon et al. [3], which were used to validate the proposed model and its ABAQUS implementation. As a result of the previous section, the following parameters have been selected for the validation Telem = 0.04 mm, DN = 500 cycles, stroke = 10 mm, and *R* = 0.5.

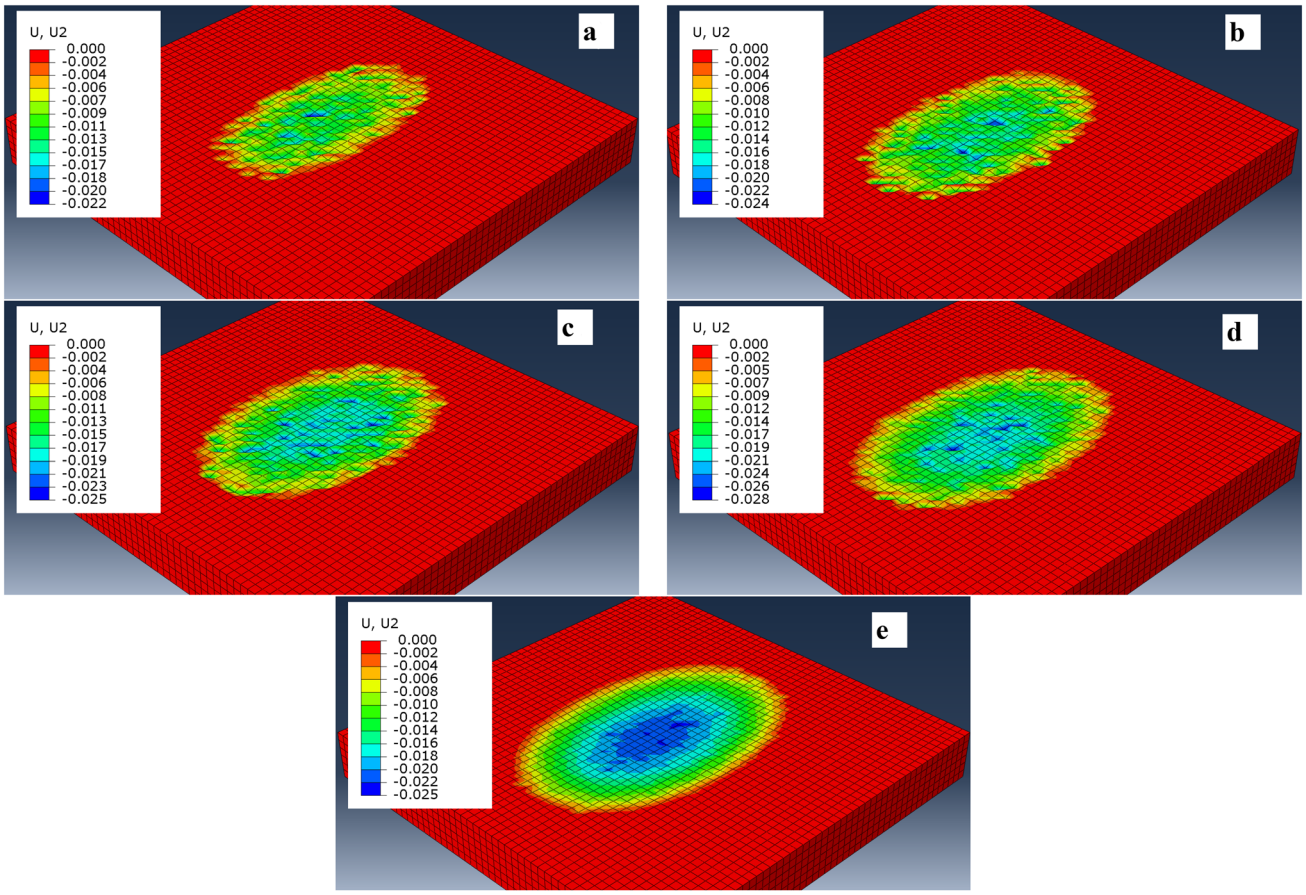


Fig. 5 Wear scar for R constant variation: **a** 1.5, **b** 1.0, **c** 0.75, **d** 0.5 and **e** 0.25

Table 1 Model validation conditions, speed = 5 mm/s. *Source* [3]

Load (N)	CoF	Specific wear rate ($mm^3/Nm) \times 10^{-6}$
5	0.84	447.4
10	0.70	369.7
20	0.76	397.3

Table 2 Contact mechanics parameter. *Source:* García-León et al. [3]

Applied load (N)	Total sliding distance (m)	Max. contact pressure (GPa)	Max. shear stress (GPa)
5	100	1.37	425.1
10		1.72	535.6
20		2.17	674.8

V. Saikko [23] and Ravikiran and Jahanmir [24]concluded that the wear rate directly depends on the apparent contact pressure. The contact parameter reported by Garcia-Leon [3] is summarized in Table 2. The maximum contact pressures found in the model are slightly lower than reported, as can be found in Table 3. The contact pressure after the initial normal load is mildly inferior to the reported one using hertz formulation in the literature, similar behavior has been reported by Sanchez et al. [25] and N. Ye and K. Komvopoulos [26].

Table 3 Contact pressure reported and modeled

Load (N)	Maximum contact pressure reported (GPa)	Model contact pressure after normal loading (GPa)
5	1.37	1.299
10	1.72	1.585
20	2.17	1.983

Figure 6a shows the Von Misses stress in a section along the stroke in the middle of the first wearing step, the peak stress, as expected, is in the contact zone, having higher values in the early steps and being reduced due to the formation of the wear scar. Peak values of Von Misses stress of

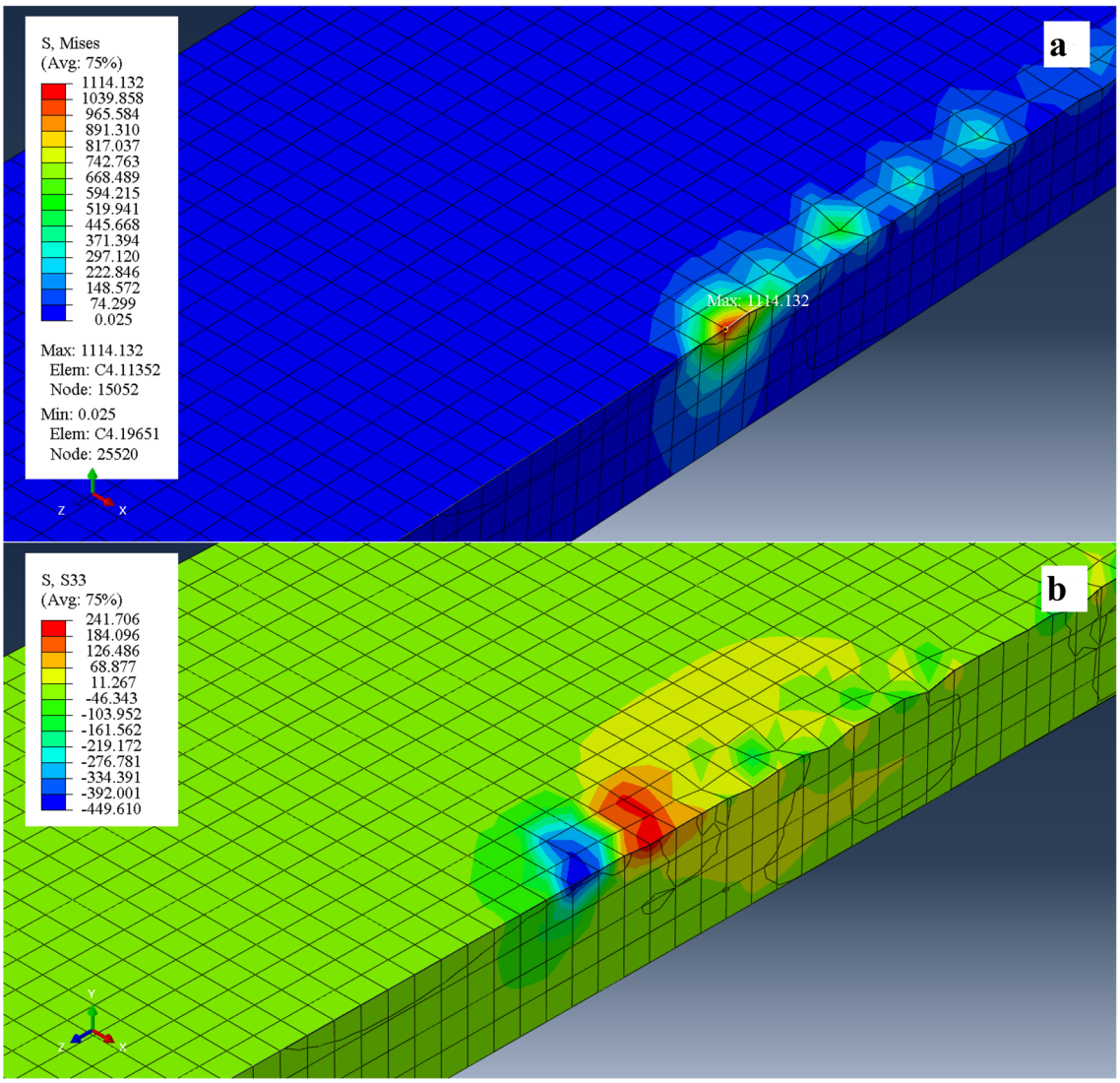


Fig. 6 **a** Von Misses stress and **b** normal stress in the direction of the stroke in a section along the stroke considering Telem = 0.04 mm, DN = 500 cycles, and $R = 0.5$ after first sliding wear

2.3 MPa with an average value of 950 MPa were found. The apparition of the residual stress and the wear scar product of the nodes movement of the mesh that simulates the wear can also be seen. In Fig. 6b, the stress on the direction of the stroke can be seen in the first wearing step; the friction force between the alumina ball and the surface creates compressive stress by the pushing force in front of the alumina ball and tensile stress behind it. Similar behavior was reported for Holmberg [5]. Due to the complexity of the contact and the continuous change of the shape of the scar, the values of the stress change along with the simulation a maximum tensile value of 644 MPa and compressive values of 1089 MPa were found, with average values around 300 MPa for tensile and 600 MPa for compressive stress. The maximum values were found at later steps on the model when the alumina ball direction changes.

The stress distribution in Fig. 6 can be considered non-accurate as the field steps are concentrated in a few nodes (more visible in the early steps of the model), but it is important to remember that it is desired to model the wear without a major computational requirement. The size of Telem and R constant can be further reduced, leading to a much more accurate stress field without major changes in the wear depth and width but with a considerable increase in the computational cost needed and leading to model instability due to the high deformation near the contact zone. Similarly, artificial roughness in the wear scar in the mesh can also be seen in Fig. 6; the artificial roughness was controlled with the implementation of the R constant and as described in Sect. 2.3,

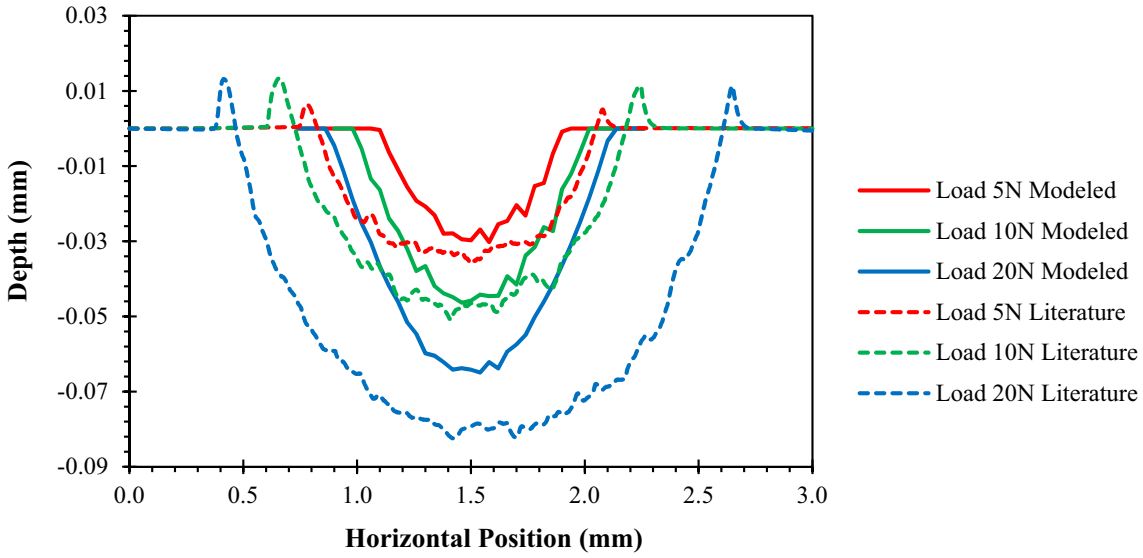


Fig. 7 Modeled and literature wear scars comparison

Table 4 Experimental and modeled wear depth comparison

Normal Load (N)	Experimental wear depth (μm)	Modeled wear depth (μm)	Percentage error (%)
5	359	297	17.20
10	509	471	7.46
20	799	649	18.77

reduced to values where its influence will be minimum in the wear scar. Further reductions of the R constant mean a lower step time that increases the number of steps needed in the model and a bigger sized file for the resulting database.

In Fig. 7, a comparison between the wear scars reported and the one obtained in the model can be found. As can be seen in the figure, the measured and predicted worn surface profiles correlate well for the wear depth, but the scar's width is mildly under-estimated behavior similar to that found by McColl et al. [12]. As can be found in Table 4, the error between the experimental and modeled wear depth is under the 18.77% error, slightly higher than the one found by Kunal and Ramkumar [13] but with a coarser mesh and without the possible controversy of using a non-axisymmetric 2D-Model to model a ball-on-flat contact. The difference between the wear scars can be attributed to non-considered variables in the model as the debris effect, alignment of the experiment, topography of the contact zone [27], temperature [28], and speed [29] (Fig. 8).

4 Conclusions

In this paper, the sliding wear behavior of a 3D ball-on-flat geometry was modeled linking a FORTRAN subroutine with ABAQUS. ALE adaptive meshing was used to maintain mesh stability and distortion control, UMESMOTION subroutine was implemented together with the Archard formulation to displace the nodes and simulate the wear of the model.

Contact element size, discretization of the number of cycles, and the maximum increasing time (represented by the R constant) were analyzed to ensure the independence of the model pressure contact and the wear depth from the mesh and minimize the computational time required. Mesh independence was found for a contact size element Telem = 0.04 mm discretization of the number of cycles DN = 500 and a relation between the element size and the stroke $R = 0.5$.

A comparison between the maximum contact pressure reported by the literature using Hertz formulation and the contact pressure at the end of the initial normal loading was made, a good agreement between the two values was found with a maximum error of 8.61% for the 20 N normal load.

The model was validated using experimental data from the literature with an alumina ball radius of 3 mm and normal load 5, 10, and 20 N with speed 5 m/s and stroke 10 mm. A comparison between the experimental data and the model

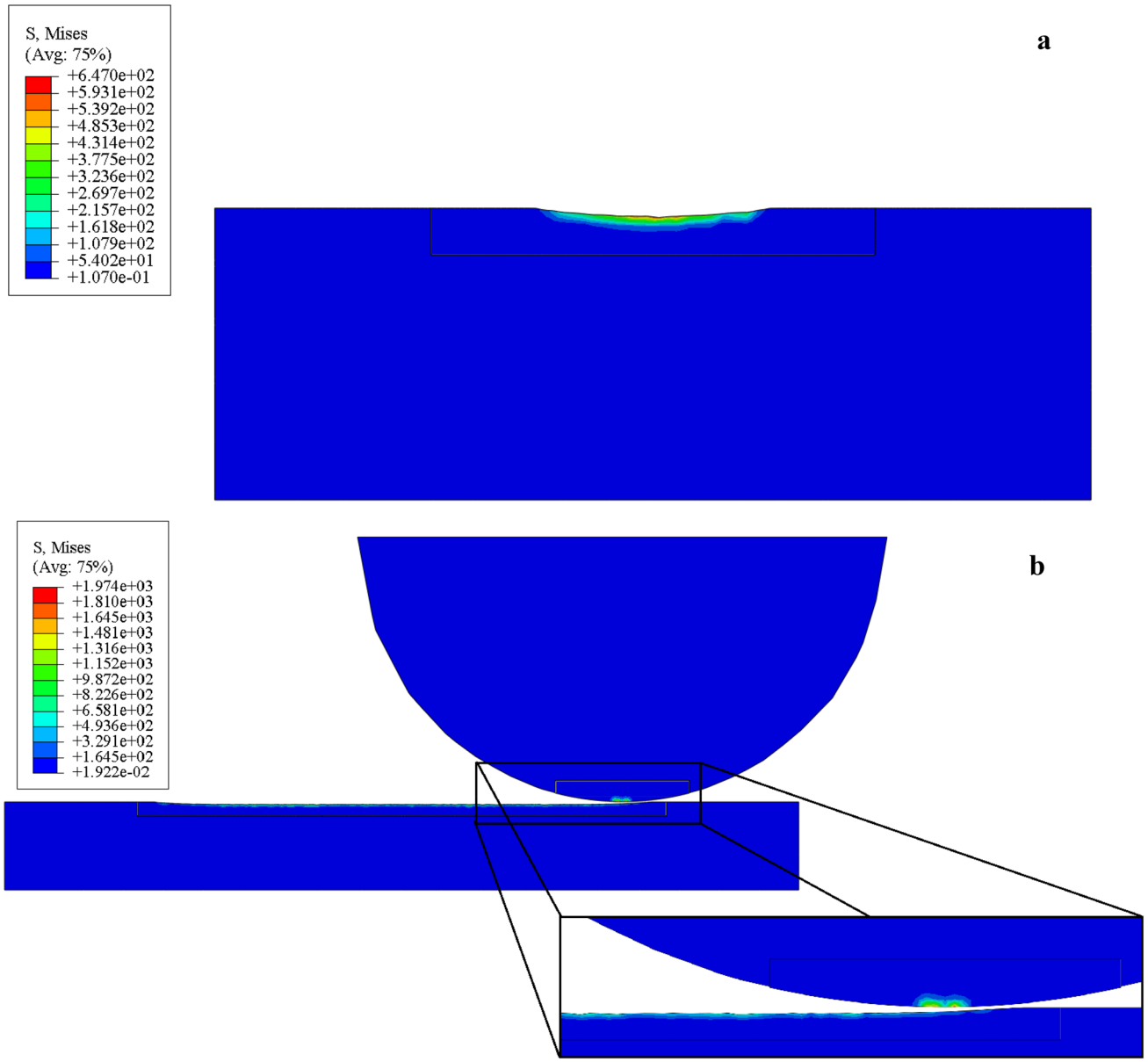


Fig. 8 **a** Residual Von Misses stress after the alumina ball retreat in a section tangential to the stroke and **b** residual Von Misses stress after the alumina ball retreat in a section in the direction of the stroke, considering Telem = 0.04 mm, DN = 500 and $K = 0.5$

was made, the modeled wear depth was slightly under-estimated with a maximum error of 18.77% for the load of 20 N.

Acknowledgements This work was supported by the research grant 20221257 of the Instituto Politécnico Nacional of México. The authors thank Eng. J. Lozano G. and KIMECA for his support on the FEM ABAQUS analysis.

References

[1] I. M. Hutchings, *Tribology: Friction and Wear of Engineering Materials*, Edward Arn. London, 1992.

[2] R. A. García-León, J. Martínez-Trinidad, I. Campos-Silva, U. Figueroa-López, and A. Guevara-Morales, "Wear maps of borided AISI 316L steel under ball-on-flat dry sliding conditions," *Mater. Lett.*, vol. 282, pp. 1–5 (128842), 2021, doi: https://doi.org/10.1016/j.matlet.2020.128842.

[3] García-León, R.A., Martínez-Trinidad, J., Guevara-Morales, A. et al. "Wear Maps and Statistical Approach of AISI 316L Alloy under Dry Sliding Conditions". *J. of Materi Eng and Perform.*, vol. 30, pp. 6175–6190, 2021, doi. https://doi.org/10.1007/s11665-021-05822-0

[4] M. P. Ananth and R. Ramesh, "Analysis of sliding behaviour of non-conformal contacting surfaces subjected to shear traction," *Procedia Eng.*, vol. 38, pp. 2645–2656, 2012, doi: https://doi.org/10.1016/j.proeng.2012.06.311.
[5] K. Holmberg, A. Laukkanen, H. Ronkainen, K. Wallin, S. Varjus, and J. Koskinen, "Tribological contact analysis of a rigid ball sliding on a hard coated surface. Part I: Modelling stresses and strains," *Surf. Coatings Technol.*, vol. 200, no. 12–13, pp. 3793–3809, 2006, doi: https://doi.org/10.1016/j.surfcoat.2005.03.040.
[6] K. Holmberg and A. Matthews, *Coatings Tribology: Properties, Mechanisms, Techniques and Applications in Surface Engineering*, Elsevier. United Kingdom, 2009.
[7] S. W. Hsu and K. C. Liao, "Wear analysis and verification of metallic terminals for electronic connectors," *Eng. Fail. Anal.*, vol. 25, pp. 71–80, 2012, doi: https://doi.org/10.1016/j.engfailanal.2012.04.010.
[8] A. P. S. Arunachalam and S. Idapalapati, "Material removal analysis for compliant polishing tool using adaptive meshing technique and Archard wear model," *Wear*, vol. 418–419, pp. 140–150, 2019, doi: https://doi.org/10.1016/j.wear.2018.11.015.
[9] V. Hegadekatte, N. Huber, and O. Kraft, "Modeling and simulation of wear in a pin on disc tribometer," *Tribol. Lett.*, vol. 24, no. 1, pp. 51–60, 2006, doi: https://doi.org/10.1007/s11249-006-9144-2.
[10] B. Kanavalli, "Application of user defined subroutine UMESHMOTION in ABAQUS for simulating dry rolling/sliding wear," p. 34, 2006.
[11] V. Hegadekatte, S. Kurzenhäuser, N. Huber, and O. Kraft, "A predictive modeling scheme for wear in tribometers," *Tribol. Int.*, vol. 41, no. 11, pp. 1020–1031, 2008, doi: https://doi.org/10.1016/j.triboint.2008.02.020.
[12] I. R. McColl, J. Ding, and S. B. Leen, "Finite element simulation and experimental validation of fretting wear," *Wear*, vol. 256, no. 11–12, pp. 1114–1127, Jun. 2004, doi: https://doi.org/10.1016/j.wear.2003.07.001.
[13] K. K. Bose and P. Ramkumar, "Finite element method based sliding wear prediction of steel-on-steel contacts using extrapolation techniques," *Proc. Inst. Mech. Eng. Part J J. Eng. Tribol.*, vol. 233, no. 10, pp. 1446–1463, 2019, doi: https://doi.org/10.1177/1350650119836813.
[14] Dassault Systèmes, "Abaqus 6.12 Online Documentation," *Notes*. 2012, doi: https://doi.org/10.1097/TP.0b013e31822ca79b.
[15] Dassault Systèmes Simulia, "Abaqus user subroutines," *Abaqus 6.12*, vol. 53, no. 9, 2013.
[16] ASM, "ASM Volume 1 Properties and Selection: Irons, Steels, and High-Performance Alloys," 1990.
[17] R. Liu and D. Y. Li, "Modification of Archard's equation by taking account of elastic/pseudoelastic properties of materials," *Wear*, vol. 250–251, no. PART 2, pp. 956–964, 2001, doi: https://doi.org/10.1016/s0043-1648(01)00711-6.
[18] K. Holmberg, H. Ronkainen, A. Laukkanen, K. Wallin, A. Erdemir, and O. Eryilmaz, "Tribological analysis of TiN and DLC coated contacts by 3D FEM modelling and stress simulation," *Wear*, vol. 264, no. 9–10, pp. 877–884, 2008, doi: https://doi.org/10.1016/j.wear.2006.12.084.
[19] J. C. Martínez, L. V. Vanegas Useche, and M. A. Wahab, "Numerical prediction of fretting fatigue crack trajectory in a railway axle using XFEM," *Int. J. Fatigue*, vol. 100, pp. 32–49, 2017, doi: https://doi.org/10.1016/j.ijfatigue.2017.03.009.
[20] M. Öqvist, "Numerical simulations of mild wear using updated geometry with different step size approaches," *Wear*, vol. 249, no. 1–2, pp. 6–11, Apr. 2001, doi: https://doi.org/10.1016/S0043-1648(00)00548-2.
[21] A. Meneses-Amador *et al.*, "Contact fatigue performance of cobalt boride coatings," *Surf. Coatings Technol.*, vol. 353, pp. 346–354, 2018, doi: https://doi.org/10.1016/j.surfcoat.2018.07.104.
[22] P. Põdra and S. Andersson, "Simulating sliding wear with finite element method," *Tribol. Int.*, vol. 32, no. 2, pp. 71–81, 1999, doi: https://doi.org/10.1016/S0301-679X(99)00012-2.
[23] V. Saikko, "Effect of contact pressure on wear and friction of ultra-high molecular weight polyethylene in multidirectional sliding," *Proc. Inst. Mech. Eng. Part H J. Eng. Med.*, vol. 220, no. 7, pp. 723–731, 2006, doi: https://doi.org/10.1243/09544119JEIM146.
[24] A. Ravikiran and S. Jahanmir, "Effect of contact pressure and load on wear of alumina," *Wear*, vol. 251, no. 1, pp. 980–984, 2001, doi: https://doi.org/https://doi.org/10.1016/S0043-1648(01)00739-6.
[25] A. Sánchez-Islas, J. Martínez-Trinidad, I. Campos-Silva, U. Figueroa-López, J. Martínez-Londoño, and R. A. García-León, "Dry Sliding Wear Test on Borided AISI 1018 Steel Under Pin-on-Disc Configuration," *Metall. Mater. Trans. A Phys. Metall. Mater. Sci.*, vol. 53, no. 1, pp. 179–199, 2022, doi: https://doi.org/10.1007/s11661-021-06511-2.
[26] N. Ye and K. Komvopoulos, "Three-dimensional finite element analysis of elastic-plastic layered media under thermomechanical surface loading," *J. Tribol.*, vol. 125, no. 1, pp. 52–59, 2003, doi: https://doi.org/10.1115/1.1497360.
[27] A. Laukkanen *et al.*, "Topographical orientation effects on surface stresses influencing on wear in sliding DLC contacts, Part 2: Modelling and simulations," *Wear*, vol. 388–389, pp. 18–28, 2017, doi: https://doi.org/10.1016/j.wear.2017.03.026.
[28] X. Zhang, K. Zhang, X. Kang, and L. Zhang, "Friction maps and wear maps of Ag/MoS2/WS2 nanocomposite with different sliding speed and normal force," *Tribol. Int.*, vol. 164, no. August, p. 107228, 2021, doi: https://doi.org/10.1016/j.triboint.2021.107228.
[29] G. Wang, G. Zhao, J. Song, and Q. Ding, "Effect of velocity and interference depth on the tribological properties of alumina sliding with Cu: A molecular dynamics simulation," *Chem. Phys. Lett.*, vol. 775, no. April, p. 138669, 2021, doi: https://doi.org/10.1016/j.cplett.2021.138669.

Publisher's Note Springer Nature remains neutral with regard to jurisdictional claims in published maps and institutional affiliations.

Springer Nature or its licensor holds exclusive rights to this article under a publishing agreement with the author(s) or other rightsholder(s); author self-archiving of the accepted manuscript version of this article is solely governed by the terms of such publishing agreement and applicable law.

View publication stats